PCCP

Accepted Manuscript

ROYAL SOCIETY OF CHEMISTRY

www.rsc.org/pccp

Structural classification of the highly disordered crystal phases of $[N_n][BF_4]$, $[N_n][PF_6]$, $[P_n][BF_4]$, and $[P_n][PF_6]$ salts (N_n^+ = tetraalkylammonium and P_n^+ = tetraalkylphosphonium)

Kazuhiko Matsumoto,[*,a] Ukyo Harinaga,[a] Ryo Tanaka,[a] Akira Koyama,[a] Rika Hagiwara,[a] and Katsuhiko Tsunashima,[b]

[a]Department of Fundamental Energy Science, Graduate School of Energy Science, Kyoto University Sakyo-ku, Kyoto 606-8501, Japan

[b]Department of Materials Science, Wakayama National College of Technology, 77 Noshima, Nada-cho, Gobo 644-0023, Japan

* E-mail: k-matsumoto@energy.kyoto-u.ac.jp

† Electronic supplementary information (ESI) available: Comments on determination of space groups, calculations of ionic radii and the radius ratio for the highly disordered phases, details on some synthetic procedures, structural data of powder and single-crystal X-ray diffraction, Raman spectroscopic data, and an X-ray diffraction image. See DOI: XXXX.XXXXX.

Abstract

The structures of 16 symmetric tetraalkylammonium (N_n^+) and tetraalkylphosphonium (P_n^+) salts ($[N_n][BF_4]$, $[N_n][PF_6]$, $[P_n][BF_4]$, and $[P_n][PF_6]$, where n = 1 to 4, and denotes the number of carbon atoms in each alkyl chain) are investigated by X-ray diffraction in order to elucidate the effect of ion size on the disordered structure of organic salts. All the salts exhibit one or more solid−solid phase transitions in differential scanning calorimetric curves. Powder X-ray diffraction revealed that the highest temperature solid phase of these salts belongs to a crystal system with high cubic or hexagonal symmetry. The structures are classified into 5 different types: CsCl', NaCl, NaCl', inverse NiAs, and $TBPPF_6$. The CsCl'-type whose octant corresponds to the original CsCl unit cell is observed for $[N_1][PF_6]$ owing to the orientational difference for the cation or anion. The NaCl-type structure is observed for the N_2^+ and P_2^+ salts while the NaCl'-type structure is observed for $[N_3][PF_6]$, where the configuration of ions is based on the NaCl-type but the four equivalent positions in the original NaCl lattice split into two sets of equivalent positions (three and one). The inverse NiAs structure is observed for $[P_3][PF_6]$. Single-crystal X-ray diffraction reveals that the disordering of ions in $[P_4][PF_6]$ becomes more significant with increasing temperature. The new structure of a cubic phase, the $TBPPF_6$-type structure, is found for the salts with long alkyl chains. The structure is roughly determined at 333 K and the ions therein are highly disordered but not rotating. The validity of the radius ratio rule is confirmed through appropriate assessment of the ion size.

Introduction

Alkylammonium and alkylphosphonium salts have been the topics of structural studies because they exhibit a variety of structural changes during thermal transitions.[1-10] Their highest temperature solid phase is particularly interesting and is characterized by disordering of the globular or pseudo-globular component ions. These phases are often referred to as ionic plastic crystals (IPCs) and have been attracting attention recently because they can be used as solid-state electrolytes in the construction of safe and reliable electrochemical devices.[11-16] Nuclear magnetic resonance studies on various alkylammonium salts have suggested that the constituent ions essentially rotate in the IPC phase.[17-22] Recent work on diethyl(methyl)(isobutyl)phosphonium hexafluorophosphate revealed that the terminal group of the cation rotates even at low temperature and rotation of the entire cation starts first as uniaxial rotation, and then tumbles isotropically at high temperatures.[23] Although isotropic rotational disordering in IPC phases is achieved by using relatively spherical anions such as BF_4^- and PF_6^-, previous literature clearly shows that even nonspherical anions such as $N(SO_2CF_3)_2^-$ also form IPC phases if combined with an appropriate cation.[24-26]

One of the prominent features of IPCs is the small entropy change of melting (ΔS_m). This originates from the highly disordered structure of the IPC whose entropy differs by only a small amount from that of the liquid phase.[1, 27, 28] Although IPCs do not always follow Timmerman's criterion for molecular plastic crystals ($\Delta S_m < 20$ J K^{-1} mol^{-1}),[29] such a small ΔS_m is often observed for tetraalkylammonium and dialkylpyrrolidnium-based IPCs.

Despite such studies on IPCs, few X-ray diffraction (XRD) studies have been performed so far for the highly disordered phase of alkylammonium salts. This may be because of the difficulty in making a detailed structural analysis through single-crystal or powder X-ray diffraction owing to the significant disordering of the component ions and large atomic displacement factors, whereas an understanding of the basic structural properties is important in applications of these materials such as their use as electrolytes. Several structural types including NaCl- and CsCl-types were identified by indexing powder diffraction patterns in the range of the highest temperature solid phase for alkylammonium salts

with halide or simple inorganic anions.[20, 30-34] Such simplification of the configuration of the component species was also observed for molecular compounds (body- or face-centered cubic) and is one of the unique characteristics of plastic crystals.[35] Although alkylpyrrolidinium and alkylpiperidinium salts of $N(SO_2CF_3)_2^-$ do not exhibit highly symmetric crystal lattices such as cubic or hexagonal, significant disordering in the high-temperature phases results in very similar and relatively simple X-ray diffraction patterns regardless of the cationic structure.[26, 36-38] Single-crystal XRD of the low-temperature phases provides some insights into the structural disordering in the high temperature solid phases. For example, alkylammonium and alkylpyrrolidinium cations show positional disordering in their low-temperature phases (e.g. $N(SO_2CF_3)_2^-$ [25, 26, 37] and BF_4^- salts[32, 39-41]), which can be regarded as the prototypical motion in high-temperature phases. It should be noted that these disordered structures observed by XRD are averaged structures and do not guarantee full and independent rotation of ions as indicated for molecular plastic crystals.[42]

The present study provides a systematic understanding of the phase behavior of 16 symmetric tetraalkylammonium (N_n^+, where n denotes the number of carbon atoms in the alkyl chain, n = 1 = methyl, n = 2 = ethyl, n = 3 = propyl, and n = 4 = butyl) and tetraalkylphosphonium (P_n^+, n = 1–4) salts with BF_4^- and PF_6^-, which fills the missing relation between the ion size and crystal structure of the highly disordered highest-temperature solid phase. The phase transition and structure of each salt is investigated through a combination of differential scanning calorimetry (DSC) and single-crystal and powder XRD.

Experimental

Chemicals. Volatile materials were handled in a vacuum line constructed of SS316 stainless steel and PFA (tetrafluoroethylene-perfluoroalkylvinylether copolymer). Nonvolatile materials were handled under a dry Ar atmosphere in a drybox. Methanol (Wako Chemicals, 99.8 %, water content < 10 ppm) for crystal growth was used as received. The tetraalkylammonium and tetraalkylphosphonium salts, $[N_1][BF_4]$ (Alfa Aesar, purity 97%), $[N_2][BF_4]$ (TCI, purity 98 %), $[N_3][BF_4]$ (Aldrich, purity 98 %),

$[N_4][BF_4]$ (Strem Chemicals, purity 99 %), $[N_1][PF_6]$ (Alfa Aesar, purity 99 %), $[N_2][PF_6]$ (Aldrich, purity 99 %), $[N_4][PF_6]$ (Fluka, purity 99 %), $[P_2][BF_4]$ (TCI, purity 95 %), $[P_4][BF_4]$ (Fluka, purity 99 %), $[P_2][PF_6]$ (TCI, purity 99 %), and $[P_4][PF_6]$ (TCI, purity 98 %) were purchased and dried under vacuum at 80 °C. Anhydrous HF (Daikin Industries) was dried over K_2NiF_6 prior to use. The tetramethylphosphonium salts, $[P_1][BF_4]$ and $[P_1][PF_6]$, were prepared by the reaction of $[P_1][(FH)_nF]$ and binary fluoride BF_3 (Nippon Sanso, purity 99.99 %) and PF_5 (Nippon Sanso, purity 99%), respectively, in anhydrous HF (Stella Chemifa Corp., purity 99.9%). The salts, $[N_3][PF_6]$, $[P_3][BF_4]$, and $[P_3][PF_6]$, were synthesized by the metathesis reaction of $[N_3]Br$ (Aldrich, purity 98 %) or $[P_3]Br$ (Nippon Chemical Industrial, purity 98 %) and the potassium fluorocomplex salts ($K[BF_4]$ (Aldrich, purity 99.99 %) and $K[PF_6]$ (Aldrich, purity 99.5 %), respectively) (See Supporting Information for the details on the synthesis of $[P_1][BF_4]$, $[P_1][PF_6]$, $[N_3][PF_6]$, $[P_3][BF_4]$, and $[P_3][PF_6]$).

Analysis. Thermogravimetric and DSC analysis was performed under a dry Ar gas flow using Shimadzu DTG-60H and Rigaku ThermoPlus EVO II DSC 8230, respectively, at the scanning rate of 5 K min^{-1}. The sample was placed in a Ni open cell for TG and in an Al sealed cell for DSC. Enthalpy changes were calculated by integrating the heat flow during each transition on the DSC curve and entropy changes were calculated by dividing the enthapy changes by the transition temperature. Density was measured using the picnometer method. The powder sample was weighed in a picnometer first and tetradecane was introduced onto it. The entire picnometer was evacuated to remove gases around the powder and tetradecane was added up to the marked line at the capillary of the picnometer. By measuring the weight of tetradecane, the density of the powder was calculated from the weights of the powder and tetradecane, the total volume, and the density of tetradecane. The density of the powder was calculated from the weight of the powder sample and its volume. Raman spectra were recorded (Nanofinder 30, Tokyo Instruments, Inc.) at room temperature using the 632.8 nm line of a He-Ne laser as the excitation line. The samples for Raman spectroscopy were loaded in Pyrex glass tubes under dry Ar and sealed with a plastic cap. Elemental analysis was performed at Organic Elemental Analysis Research Center, Kyoto University. Powder X-ray diffraction patterns were recorded using Ultima IV

X-ray diffractometer (Rigaku Corp.) equipped with a scintillation counter detector and graphite-monochromated Cu-Kα irradiation (1.5418 Å; 40 kV−40 mA). The well-ground sample spread on a Cu holder was placed in a temperature controlling apparatus. The measurement was performed under vacuum with a scanning rate of 0.1° min^{-1}. The obtained data was indexed by DICVOL06 with zero-point correction.[43] Single-crystal X-ray diffraction data were collected on R-axis Rapid II diffractometer (Rigaku Corp.) equipped with an imaging plate area detector (using the program RAPID XRD 2.3.355) and graphite-monochromated MoKα radiation (0.71073 Å; 50 kV-40 mA). Crystals of $[P_4][PF_6]$ for low temperature data collection were grown by slow recrystallization of a saturated methanol solution from 258 to 233 K. The supernatant methanol solution was removed with pipette and the residual methanol was removed by dry Ar flow for 2 h at 233K. Suitable crystals were selected under a cold nitrogen stream (< 223 K) to avoid possible solid-solid phase transition. A selected crystal measuring 0.2x0.2x0.6 mm^3 was picked up with a glass pin under a dry nitrogen flow (below 223 K) and mounted to a goniometer head, using the cryotongs. A crystal of $[P_4][PF_6]$ measuring 0.1x0.1x0.1 mm^3 for high temperature data collection was grown in a quartz capillary by slow solidification from the liquid phase. Data collection at 113, 243, and 273 K consisted of 12 ω scans (130−190° and 5° $frame^{-1}$) at fixed φ (0°) and χ (45°) angles and 32 ω scans (0−160° and 5° $frame^{-1}$) at fixed φ (180°) and χ (45°) angles. Data collection at 333 K consisted of 36 ω scans (0−180° and 5° $frame^{-1}$) at fixed φ (30°) and χ (45°) angles and 36 ω scans (0−180° and 5° $frame^{-1}$) at fixed φ (210°) and χ (45°) angles. The exposure times were 500 s deg^{-1} at 113, 243, and 273 K and 900 s deg^{-1} at 333 K. Integration, scaling, and absorption corrections were performed using RAPID AUTO 2.40.[44] The structure was solved using SIR-92[45] and refined by SHELXL-97[46] linked to Win-GX.[47] Anisotropic displacement factors were introduced for all atoms for the refinement of the data at 113, 243, and 273 K. Displacement factors were isotropically determined in the case of the data at 333 K because of the highly disordered structure. Hydrogen atoms were determined using an appropriate riding model for the data at 113, 243, and 273 K and were not determined for the data at 333 K.

Results and discussion

Thermal properties. Thermogravimetric curves of the N_n^+ and P_n^+ salts are shown in Figure 1. For $[N_n][BF_4]$, the introduction of a long alkyl chain makes the salt thermally less stable, which agrees with the trend shown in previous works,[2, 48] which also applies to $[N_n][PF_6]$. The $[N_n][BF_4]$ salt is thermally less stable than the $[P_n][BF_4]$ salt with the same alkyl chain lengths. Some of the $[P_n][BF_4]$ salts, $[P_2][BF_4]$ and $[P_3][BF_4]$ exhibit two step decomposition curves, whereas a similar but weak trend was observed for $[N_2][BF_4]$. The distortion of the TG curve for $[N_1][BF_4]$ arises from its highly exothermic decomposition reaction. The $[P_1][PF_6]$, $[P_2][PF_6]$, and$[P_3][PF_6]$ salts exhibit distinct two-step decomposition curves, whereas the decomposition of $[P_4][PF_6]$ follows a one-step

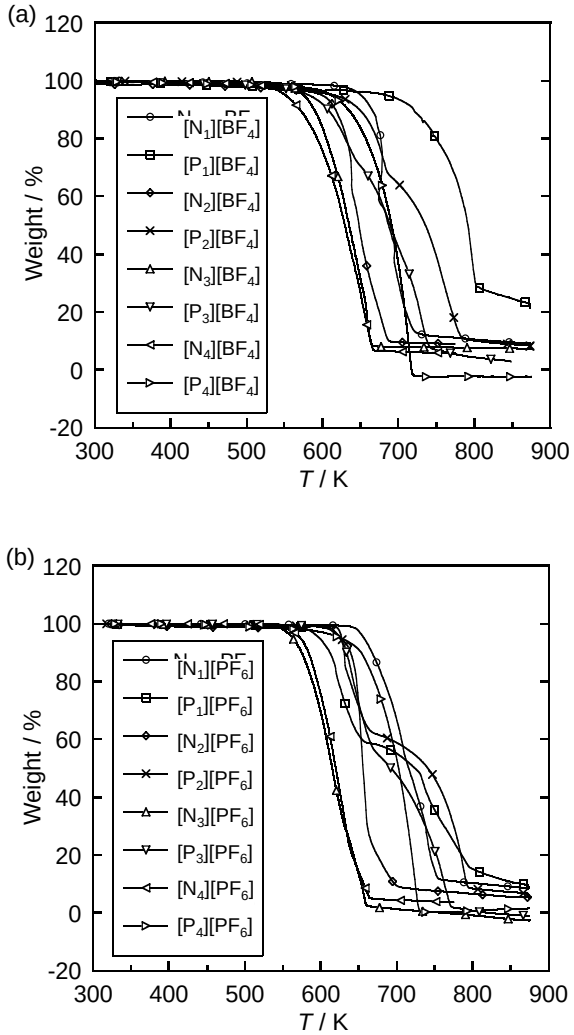

Figure 1. Thermogravimetric curves for (a) $[N_n][BF_4]$ and $[P_n][BF_4]$ and (b) $[N_n][PF_6]$ and $[P_n][PF_6]$. Scan rate: 5 K min^{-1}.

pathway similar to that of $[P_4][BF_4]$. According to the results differential thermal analysis combined with thermogravimetric analysis, the N_1^+, N_2^+, P_1^+, and P_2^+ salts exhibit signs of decomposition without melting or around their melting temperature in the heating scan (see Figure S1, Supporting Information, for the results of differential thermal analysis).

Details of the thermal transitions were investigated by DSC. The DSC curves during the heating scan for the N_n^+ and P_n^+ salts are shown in Figure 2 (see Figure S2, Supporting Information, for the full DSC curves). The transition temperature, ΔH, and ΔS of each transition are listed in Table 1. All the N_n^+ and P_n^+ salts show one or more solid−solid phase transitions. In this paper, the solid phases observed are called Phases I, II, III, and IV, from the highest-temperature phase to the lowest. The exceptions are $[P_1][BF_4]$ and $[P_1][PF_6]$; in these cases, the highest temperature-solid phase is called Phase II, and an imaginary Phase I is introduced because the structure of the highest solid phases with high-symmetry crystal lattices could not be confirmed by powder XRD below their decomposition temperatures. Although the crystal structure of the highest-temperature solid phase for $[N_1][BF_4]$ was also unidentified, it is called Phase I by analogy with $[N_1][PF_6]$ (see the section on structural analysis below for discussion).

A comparison with previous reports on the phase transitions of $[N_n][BF_4]$,[1, 2, 49] showed the following two observations. First the weak transition peak at 289 K for $[N_3][BF_4]$ reported in the previous works is not observed in the present study, possibly because of the difference in thermal history. Second, two transition peaks at 256 and 314 K in the DSC curve of $[N_4][BF_4]$, which were not reported in previous works, are observed in the present work. The DSC curve of $[N_1][PF_6]$ is similar to that of $[N_1][BF_4]$ but the solid−solid phase transition temperature is 61 K lower. The $[N_2][BF_4]$ and $[N_2][PF_6]$ salts show very similar thermal behaviors and only one solid−solid transition (338 K for $[N_2][BF_4]$ and 342 K for $[N_2][PF_6]$). The phosphonium analogues show different phase behaviors. Four solid phases are observed for $[P_1][BF_4]$, whereas only two solid phases are found for $[P_1][PF_6]$ (the imaginary phase is not included here). The thermal behavior of $[P_2][BF_4]$ is similar to that of $[P_2][PF_6]$. Both the solid−solid phase transition temperatures from Phase III to Phase II and from Phase II to Phase I of $[P_2][BF_4]$

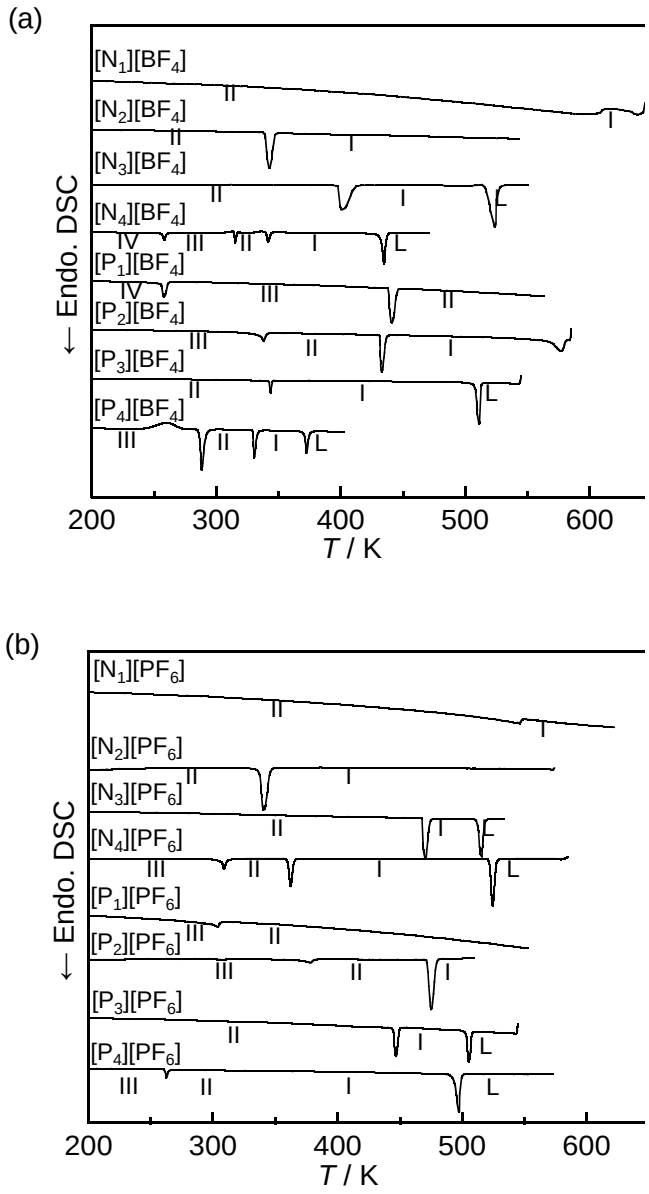

Figure 2. Differential scanning calorimetric curves obtained during the heating scan for (a) $[N_n][BF_4]$ and $[P_n][BF_4]$ and (b) $[N_n][PF_6]$ and $[P_n][PF_6]$. Scan rate: 5 K min^{-1}.

(338 and 425 K, respectively) are lower than those of $[P_2][PF_6]$ (373 and 474 K, respectively). All the N_3^+, P_3^+, N_4^+, and P_4^+ salts exhibit two or more solid−solid phase transitions due to the large conformational freedom of the alkyl chains, and melt below their decomposition temperatures.

Table 1. Summary of thermal behavior for $[N_n][BF_4]$, $[N_n][PF_6]$, $[P_n][BF_4]$, and $[P_n][PF_6]$.[a]

	Transition	T / K	ΔH / kJ mol^{-1}	ΔS / J K^{-1} mol^{-1}
$[N_1][BF_4]$	II → I	606	0.18	0.30
	T_d	651	–	–
$[P_1][BF_4]$	IV → III	256	1.5	5.9
	III → II	439	4.9	11.1
	II → I	–	–	–
	T_d	685		
$[N_2][BF_4]$	II → I	342	8.2	23.9
	T_d	606	–	–
$[P_2][BF_4]$	III → II	338	1.6	4.6
	II → I	425	7.7	18.2
	I → L	577	4.0	6.9
	T_d	616		
$[N_3][BF_4]$	II → I	402	9.3	23.1
	I → L	521	8.9	17.1
	T_d	575	–	–
$[P_3][BF_4]$	II → I	343	1.6	4.6
	I → L	509	12.1	23.6
	T_d	582	–	–
$[N_4][BF_4]$	IV → III	256	1.6	6.3
	III → II	314	1.2	3.7
	II → I	340	2.1	6.1
	I → L	432	8.7	20.2
	T_d	551	–	–
$[P_4][BF_4]$	III → II	284	24.1	84.7
	II → I	329	6.9	20.8
	I → L	368	6.4	17.4
	T_d	612	–	–
$[N_1][PF_6]$	II → I	545	0.13	0.24
	T_d	657		
$[P_1][PF_6]$	III → II	302	0.12	0.39
	II → I	–	–	–
	T_d	599	–	–
$[N_2][PF_6]$	II → I	338	7.2	21.3
	T_d	627	–	–
$[P_2][PF_6]$	III → II	373	1.0	2.8
	II → I	474	12.9	27.3
	T_d	606	–	–
$[N_3][PF_6]$	II → I	473	10.8	22.8
	I → L	516	8.6	16.6
	T_d	563	–	–
$[P_3][PF_6]$	II → I	445	5.7	12.8
	I → L	504	5.8	11.5
	T_d	616	–	–
$[N_4][PF_6]$	III → II	307	5.2	16.9
	II → I	360	9.5	26.5
	I → L	522	15.7	30.1
	T_d	573	–	–
$[P_4][PF_6]$	III → II	258	0.91	3.3
	(II→ I)[b]	–	–	–
	I → L	490	10.3	21.0
	T_d	627	–	–

[a] Solid-solid and solid-liquid transition temperatures were determined by DSC. Decomposition temperature (T_d) was determined as that at 5 % weight loss in TG curves. Roman numerals (I, II, III, and IV) and "L" in the Transition column denote each solid phase and liquid phase in Figure 2. [b]This transition was observed only by single-crystal XRD.

Structural analysis by powder X-ray diffraction. The powder X-ray diffraction patterns of the N_n^+ and P_n^+ salts were measured at the temperature corresponding to each phase in the DSC results. The temperature dependence of the powder XRD patterns for $[P_2][PF_6]$ is shown in Figure 3 as an example and the others are shown in Figures S3−S16 (Supporting Information). In most cases, changes in the diffraction patterns correspond to the phase transitions observed in the DSC curves in Figure 2. The general trend observed is the decrease in the number of diffraction peaks with increasing temperature because the higher temperature phase tends to belong to a lattice with higher symmetry. The powder XRD patterns of Phase I for the N_n^+ and P_n^+ (n = 2, 3, and 4) salts are shown in Figure 4. The observed diffraction peaks are listed in Table S1 (Supporting Information). The structural types obtained by indexing the XRD patterns are summarized in Table 2 and the calculated diffraction peaks are listed in Table S1 (comparison between the observed and calculated peak positions are shown in Figures S17−S19, Supporting Information). Detailed structural refinement of Phase I for the present salts was impossible except for the $TBPPF_6$-type structure described below due to the significant disordering. Thus, the structural types are discussed based on powder diffraction only by indexing. The extinction rules and formula unit volume (*FUV*) for the present salts allow only the simple structures known for inorganic salts by considering the multiplicity of each site. The structures of Phase I for the present salts are classified into 5 different structures including one body-centered cubic, one face-centered cubic, two primitive cubic, and one hexagonal lattices. The details of these structures are discussed below.

The X-ray diffraction patterns of $[N_1][BF_4]$ (Phase II, Figure S3), $[P_1][BF_4]$ (Phase III, Figure S4), $[N_1][PF_6]$ (Phase II, Figure 5), and $[P_1][PF_6]$ (Phase III, Figure S5) at 298 K resemble each other, suggesting their structures are similar to each other and considered to be based on the ion configuration in the previously known $[N_1][PF_6]$ structure as described below. Phase I of $[N_1][PF_6]$ has a cubic lattice, whereas $[P_1][BF_4]$ and $[P_1][PF_6]$ decompose at elevated temperatures without forming a high-symmetry crystal lattice.[50] The temperature range of Phase I for $[N_1][BF_4]$ was out of the range of our temperature controller for XRD, and its structure was not investigated in the present study. The crystal structure of $[N_1][PF_6]$ determined at 170 K in a previous study belongs to a tetragonal system (space group

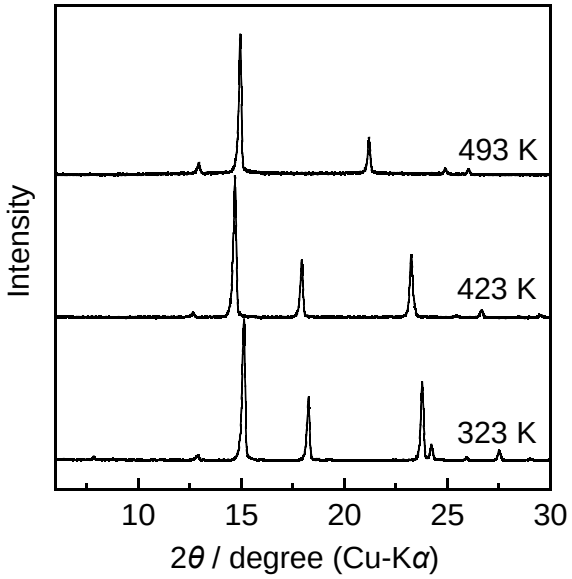

Figure 3. X-ray diffraction patterns of $[P_2][PF_6]$ at 323 K (Phase III), 423 K (Phase II), and 493 K (Phase I).

Table 2. Structural types (crystal system, space group, and lattice parameters) of Phase I for $[N_n][BF_4]$, $[P_n][BF_4]$, $[N_n][PF_6]$, and $[P_n][PF_6]$[a]

	BF_4^-	PF_6^-
N_1^+	–	CsCl' at 563 K, a = 12.59(2), V = 1997(5) Å^3, Z = 8
N_2^+	NaCl at 373 K, a = 10.827(6) Å, V = 1269.2(12) Å^3, Z = 4	NaCl at 373 K, a = 11.309(2) Å, V = 1446.3(4) Å^3, Z = 4
N_3^+	$TBPPF_6$ at 453 K, a = 14.129(6) Å, V = 2820(2) Å^3, Z = 6	NaCl' at 493 K, a = 12.047(16) Å, V = 1748(4) Å^3, Z = 4
N_4^+	$TBPPF_6$ at 413 K, a = 14.971(8) Å, V = 3353(3) Å^3, Z = 6	$TBPPF_6$ at 413 K, a = 15.3538(13) Å, V = 3619.5(5) Å^3, Z = 6
P_1^+	–	–
P_2^+	NaCl at 473 K, a = 11.331(11) Å, V = 1455(2) Å^3, Z = 4	NaCl at 498 K, a = 11.845(2) Å, V = 1661.7(5) Å^3, Z = 4
P_3^+	$TBPPF_6$ at 423 K, a = 14.298(6) Å, V = 2923(2) Å^3, Z = 6	Inverse NiAs at 473 K, a = 9.702(4) Å, c = 12.9888(11) Å, V = 1050.7(11) Å^3, Z = 2
P_4^+	$TBPPF_6$ at 348 K, a = 15.097(8) Å, V = 3440(3) Å^3, Z = 6	$TBPPF_6$ at 338 K, a = 15.315(7) Å, V = 3592(3) Å^3, Z = 6

[a] CsCl'-type structure: CsCl-type structure but the ions have different orientation and the cell is eight times larger than that for the typical CsCl type structure. NaCl: NaCl-type structure, NaCl': NaCl-type structure but the ions have different orientation, Inverse-NiAs: inverse NiAs-type structure, $TBPPF_6$: a cubic structure represented by Phase I of tetrabutylphosphonium hexafluorophosphate, $[P_4][PF_6]$.

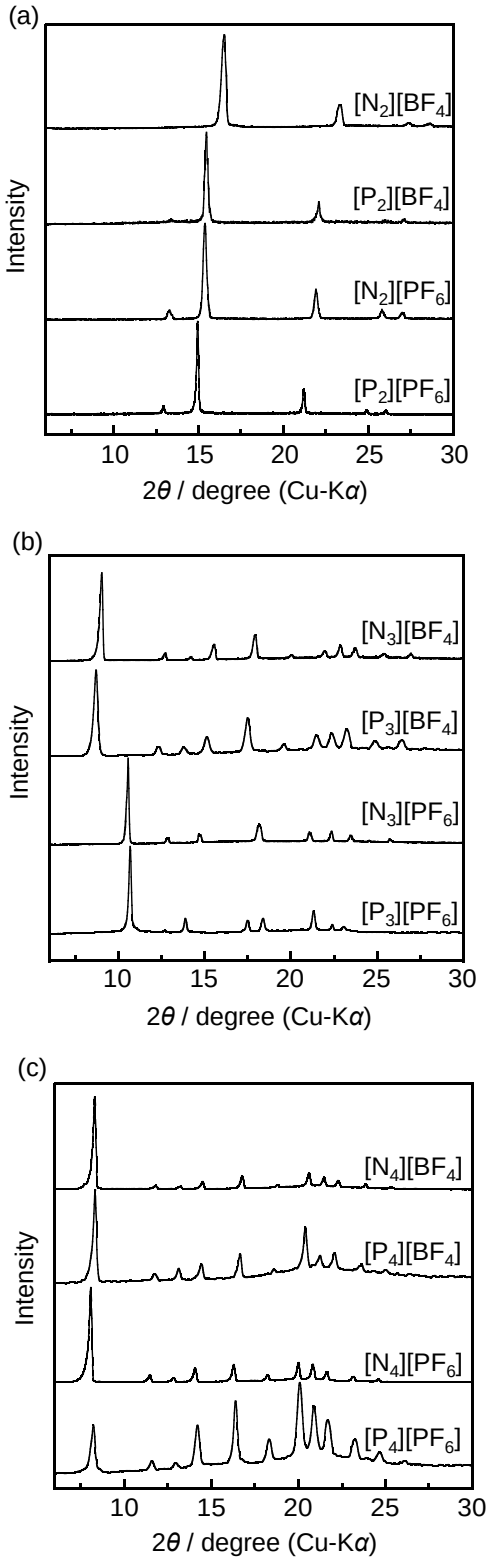

Figure 4. X-ray diffraction patterns of Phase I for (a) $[N_2][BF_4]$ at 373 K, $[P_2][BF_4]$ at 473 K,$[N_2][PF_6]$ at 373 K, and $[P_2][PF_6]$ at 498 K, (b) $[N_3][BF_4]$ at 453 K, $[P_3][BF_4]$ at 423 K,$[N_3][PF_6]$ at 493 K, and $[P_3][PF_6]$ at 473 K, and (c) $[N_4][BF_4]$ at 413 K, $[P_4][BF_4]$ at 348 K, $[N_4][PF_6]$ at 413 K, and $[P_4][PF_6]$ at 338 K.

*P*4/*nmm*, a = 8.436 Å, c = 6.089 Å, Z = 2).[51] The powder XRD patterns of $[N_1][PF_6]$ at 563, 473, 373, and 298 K are shown in Figure 5 together with the simulated XRD pattern at 170 K. Although the XRD pattern of $[N_1][PF_6]$ at 298 K can be indexed as a tetragonal lattice (a = 8.625(10) Å, c = 6.227(8) Å, Z = 2) and there are some differences between this XRD pattern and the simulated XRD pattern for the structure at 170 K such as the peak intensities of the three relatively strong peaks in the 2θ region between 14 and 21° and the new peaks in the observed pattern at 30.82 and 34.64° (Table S2, Supporting Information), suggesting that a structural transformation occurs between 170 and 298 K. This transformation may correspond to the small transition observed in the DSC curve (Figure S2). The unit cell of the low-temperature phase for $[N_1][PF_6]$ is shown in Figure 6. Although the ordered cation and anion roughly adopt a CsCl-type configuration in this structure, the two ordered PF_6^- anions are located alternately up and down along the (110) direction to minimize the approach of the methyl group of N_1^+. Some XRD peaks splitting at 298 K gradually get closer to each other with increasing

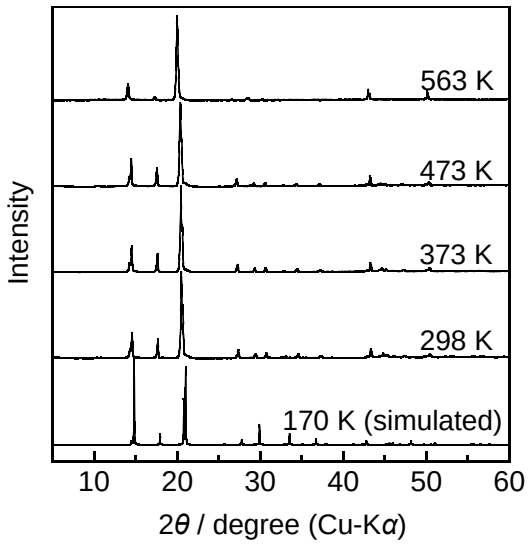

Figure 5. X-ray diffraction patterns of $[N_1][PF_6]$ at 298, 373, 473, and 563 K. The simulated pattern at 170 K from the single-crystal XRD data is also shown.[51]

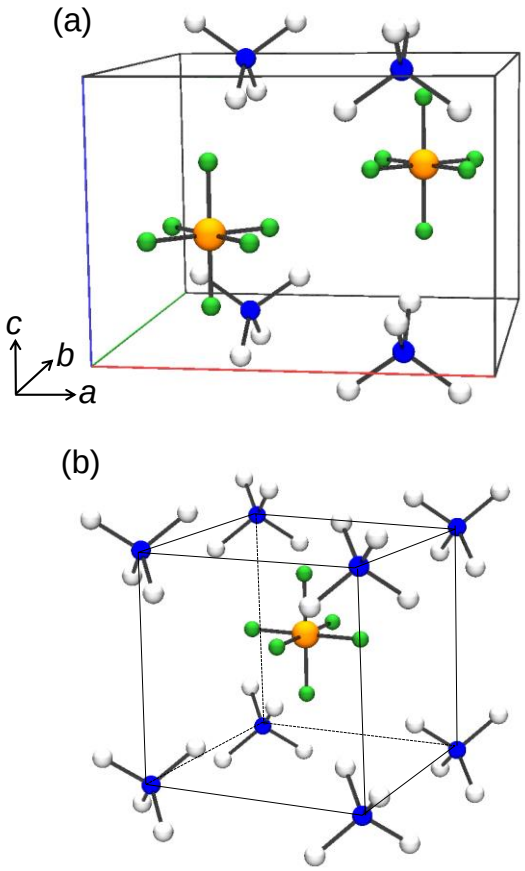

Figure 6. Crystal structure of $[N_1][PF_6]$ at 170 K:[51] (a) unit cell and (b) pseudo CsCl-type cell. The N···N direction in the pseudo CsCl-type cell corresponds to the (110) direction in the unit cell. The z values in the atomic coordinates for the P atoms in the unit cell are 0.4119 and 0.5881. Hydrogen atoms are omitted for clarity.

temperature and unite at 563 K in Phase I. The XRD pattern at 563 K is indexed as a cubic lattice with *a* = 12.59(2) Å and *V* = 1997(5) Å^3, and the extinction rule is consistent with the centrosymmetric space group *Im*-3*m* and non-centrosymmetric space groups *I*−43*m* and *I*432. Considering the *FUV* of $[N_1][PF_6]$ at 170 K (216.7 Å^3) and 298 K (231.6 Å^3), *Z* at 563 K is determined to be eight. Lattice parameter *a* of 12.59(2) Å in the structure at 563 K is slightly larger than twice the N···N distances in the distorted CsCl structure at 170 K (5.965 Å and 6.089 Å), which suggests that the crystal structure of $[N_1][PF_6]$ at 563 K is a superlattice with a doubled cell constant of the original CsCl-type lattice which is now an octant of the unit cell. This can occur for the centrosymmetric space group *Im*-3*m* when the 2*a* [(0,0,0) and (1/2, 1/2, 1/2)] and 6*b* [(1/2, 1/2, 0), (1/2, 0, 1/2), (0, 1/2, 1/2), (0, 0, 1/2), (0, 1/2, 0), and

(1/2, 0, 0)] sites of the like ions are distinguished from each other owing to orientational differences. The other ions are located at the 8*a* site [(1/4, 1/4, 1/4), (1/4, 1/4, 3/4), (1/4, 3/4, 1/4), (3/4, 1/4, 1/4), and their (1/2, 1/2, 1/2) translated positions]. Similar discussions are possible for the non-centrosymmetric space groups, *I*432 and *I*-43*m* (see Supporting Information S-1). This structural type is called the CsCl'-type in this study (Figure 7).

The X-ray diffraction patterns of Phase I for $[N_2][BF_4]$, $[P_2][BF_4]$, $[N_2][PF_6]$, and $[P_2][PF_6]$ are shown in Figure 4(a), and are indexed as a cubic lattice. The extinction rule suggests they belong to a face-centered lattice with the centrosymmetric space group *Fm*−3*m* or non-centrosymmetric groups *F*432 and *F*−43*m*. The *FUV*s determined for $[N_2][BF_4]$ at 298 K and $[N_2][PF_6]$ at 220 K above are 294.5 and 316 $Å^3$, respectively, whereas the *V* parameters of $[N_2][BF_4]$ and $[N_2][PF_6]$ at 373 K are 1269.2(12) and 1446.3(4) $Å^3$, respectively. Considering the lattice expansion in forming plastic crystal lattices as in the case of $[N_1][PF_6]$, *Z* of Phase I for $[N_2][BF_4]$, $[P_2][BF_4]$, $[N_2][PF_6]$, and $[P_2][PF_6]$ is determined to be 4, and their basic ion configuration is the NaCl-type structure in any of the possible three space groups, with the cations and anions occupying 4*a*[(0, 0, 0), (1/2, 1/2, 0), (1/2, 0, 1/2), and (0, 1/2, 1/2)] and 4*b*[(1/2, 1/2, 1/2), (1/2, 0, 0), (0, 1/2, 0), and (0, 0, 1/2)] sites, respectively (Figure 7).

A variety of structures are observed for Phase I of the $N_3^+$and P_3^+ salts, whose XRD patterns are shown in Figure 4(b). The X-ray diffraction pattern of $[N_3][PF_6]$ is indexed as a cubic lattice with a = 12.047(16) Å, which is greater than that of $[N_2][PF_6]$ (11.309(2) Å) with a smaller cation. The *FUV* of the low temperature phase of $[N_3][BF_4]$ is 397 $Å^3$;[39] therefore, *Z* of this lattice is estimated to be 4 (note that the difference between BF_4^- and PF_6^- is negligible in the rough estimation of *Z*). However, the observed indices violate the extinction rule for the NaCl-type structure, and suggest the centrosymmetric space group *Pm*−3*m* and the non-centrosymmetric space groups *P*−43*m* and *P*432. In these space groups, the cation occupies the 1*a* [(0, 0, 0)] and 3*c* sites [(1/2, 1/2, 0), (1/2, 0, 1/2), and (0, 1/2, 1/2)], and the anion occupies the 1*b* [(1/2, 1/2, 1/2] and 3d sites [(1/2, 0, 0), (0, 1/2, 0), and (1/2, 1/2, 0)] (or vice versa). In other words, the 4*a* and 4*b* sites in *Fm*−3*m* are divided into 1*a* and 3*c* and into 1*b* and 3*d* sites, respectively, unlike in the NaCl-type structure. This is probably caused by the difference in orientation

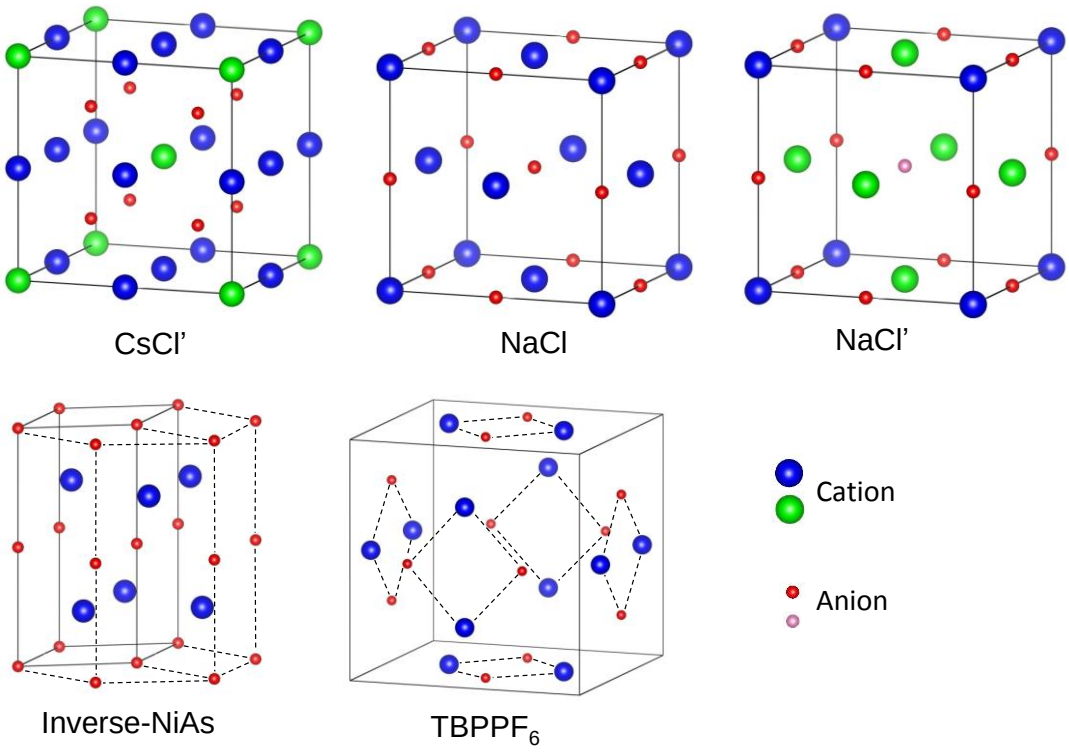

Figure 7. Schematic drawings of Phase I structures, CsCl', NaCl, NaCl', inverse NiAs, and $TBPPF_6$. The central positions of the cation and anion are shown in these structures. For the $TBPPF_6$-type structure, the ions are regarded to be highly disordered but not pseudo-spherical as shown in Figure 8.

of the ion at these sites. The difference between the centrosymmetric and non- centrosymmetric space groups is not clear in the present analysis, but arises from the difference in site symmetry; the configuration of alkyl chains or F atoms may lower the molecular symmetry and result in lower site symmetries that do not satisfy the one in the centrosymmetric space group. This structural type is called the NaCl'-type in this study (Figure 7). The X-ray diffraction pattern of $[P_3][PF_6]$ is indexed as a hexagonal lattice with a = 9.702(4) Å, c = 12.9888(11) Å, and V = 1050.7(11) $Å^3$. The Z value is estimated to be 2 through comparison with the *FUV* of the low-temperature phase of $[N_3][BF_4]$ (397 $Å^3$).[39] Two hexagonal lattices with Z = 2 are known as typical structural types for 1:1 salts: wurtzite- (space group: $P6_3mc$) and NiAs- (space group: $P6_3/mmc$) types, whereas the present NiAs structure should be called the inverse NiAs-type because the cation is larger than the anion. The tetrahedral site in the wurtzite structure has a smaller space than the octahedral site in the inverse NiAs structure. The

extinction rule of the X-ray diffraction indices matches both the space groups. Christe et al. mentioned that the *c*/*a* ratio can be an indicator for distinguishing the two structures; the *c*/*a* values are 1.63 for the wurtzite structure and 1.39 for the NiAs structure.[52] The *c*/*a* ratio of $[P_3][PF_6]$ is 1.33, which is close to the value for the NiAs structure. Thus, $[P_3][PF_6]$ is considered to belong to the inverse NiAs-type structure (Figure 7) (the radius ratio rule discussed below also confirms the inverse NiAs structure). To our knowledge, there are two examples of organic salts with this structural type: $[P_2][(FH)_2F]$[53] and $[N_1]F$.[52] The $[N_3][BF_4]$ and $[P_3][BF_4]$ salts belong to a primitive cubic lattice as in the cases of the N_4^+ and P_4^+ salts; details of this structure are discussed below. In the NaCl'-type and inverse NiAs-type structures, the thermal motions of the ions are considered to be very large and the ions are highly disordered at least to satisfy the high site symmetry.

The X-ray diffraction patterns of $[N_4][BF_4]$, $[P_4][BF_4]$, $[N_4][PF_6]$, and $[P_4][PF_6]$ shown in Figure 4(c) are indexed as cubic lattices. The extinction rule suggests they belong to a primitive cubic lattice with the centrosymmetric space group $Pm\bar{3}n$ or the non-centrosymmetric space group $P\bar{4}3n$. Although a similar pattern was reported in a previous work for $[N_4]I$ at 400 K indexed as a cubic cell,[54] there has been no further discussion so far. The details of this structure are provided in the next section.

Structural changes of $[P_4][PF_6]$ along the phase transitions. The structural changes of $[P_4][PF_6]$ along the phase transitions were studied by single-crystal XRD as an example of the salts that have Phase I with the primitive cubic lattice mentioned above ($[N_3][BF_4]$, $[P_3][BF_4]$, $[N_4][BF_4]$, $[P_4][BF_4]$, $[N_4][PF_6]$, and $[P_4][PF_6]$) (see Table S3, Support ing Information, for detailed crystallographic data). The ORTEP diagrams of the structures at 113, 243, 273, and 333 K are shown in Figure 8. The structure determined at 113 K belongs to a monoclinic space group of $P2_1/c$, and is isostructural with the known $[N_4][PF_6]$ structure at 110 K.[55] The asymmetric unit of $[P_4][PF_6]$ at 113 K contains a cation/anion pair. Three of the four butyl chains in P_4^+ adopt an all-trans conformation, while the one with P−C−C−C and C−C−C−C torsion angles of 173.01(11)° and −68.09(18)° does not. The PF_6^- anion is ordered at this temperature with a nearly ideal octahedral geometry. Although the unit cell at 243 K still belongs to the

space group $P2_1/c$, PF_6^- is disordered around two F−P−F axes. On the other hand, P_4^+ is ordered at this temperature with larger atomic displacement factors than at 113 K. Upon warming to 273 K, the solid−solid transition occurs as shown in the DSC curve, and the crystal transforms from monoclinic to orthorhombic (space group: *Pmcn*), that is, the β angle in the monoclinic cell reaches 90° at the transition temperature. The three-dimensional disordering of PF_6^- leads to its almost spherical behavior. Significant disordering with large atomic displacement factors is also observed for P_4^+, but it does not look like a spherical rotation of the entire ion. Although the crystal lattice of $[P_4][PF_6]$ at 298 K belongs to the orthorhombic cell with slightly larger cell lengths than at 273 K, the crystal broke into pieces at 323 K, suggesting a phase transition to the cubic phase. Although the reason for the discrepancy in the DSC and single-crystal XRD behaviors is not yet clear, one of the most probable reasons is the difference in the behaviors of the powder and single-crystal samples. The powder XRD pattern at 298 K is similar to that of Phase I (even after cooling to 233 K) and does not match the results of single-crystal XRD either. Figure 9 shows the changes in lattice parameters (*a*, *b*, *c*, β, and *V*) with increasing temperature. Parameters *a* and *c* increase and *b* decreases with increasing temperature.

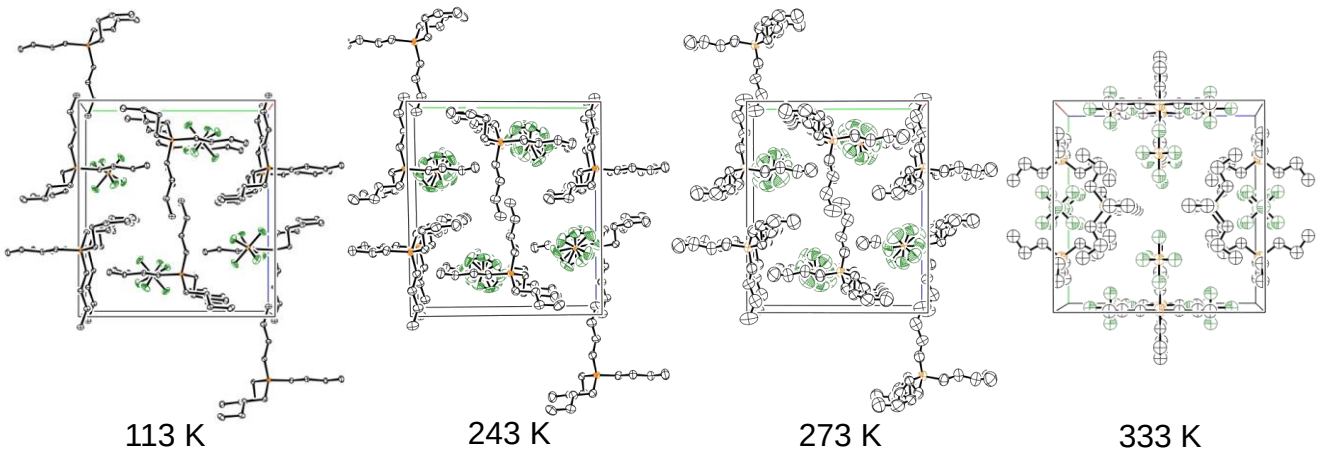

Figure 8. ORTEP diagrams of the unit cell for $[P_4][PF_6]$ at 113, 243, 273, and 333 K. Hydrogen atoms are omitted for clarity. Thermal ellipsoids are shown at the 50% probability level for the structures at 113, 243, and 273 K, and at the 5% probability level for the structure at 333 K. The structure at 333 K was not fully refined owing to the significant disordering of the component ions.

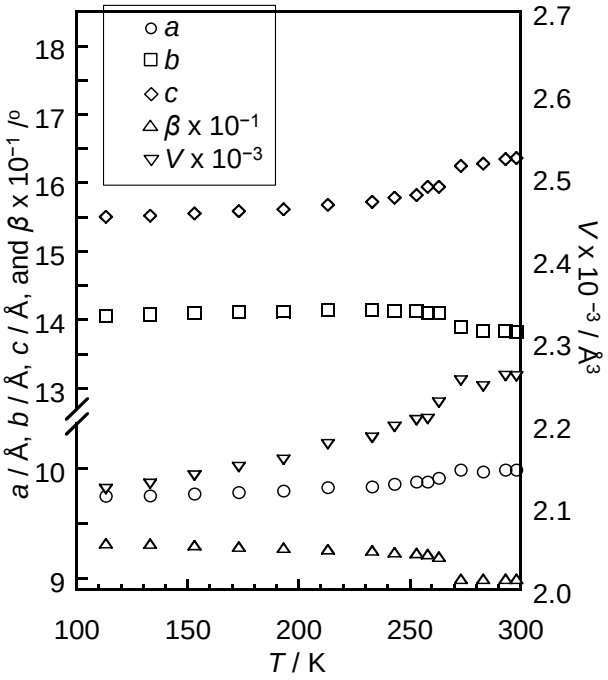

Figure 9. Temperature dependence of the *a*, *b*, *c*, *β*, and *V* lattice parameters for $[P_4][PF_6]$ determined by single-crystal XRD.

Parameter *β* decreases as the temperature approaches the transition temperature and drops to 90 near the temperature of the transition to the orthorhombic phase. The change in *V* is relatively monotonous in the temperature range of the monoclinic cell, and a gap is observed at the transition temperature to the orthorhombic cell. The thermal expansion in the monoclinic cell is 4.7% during the temperature change from 113 to 298 K, which is in the range 3−7% proposed recently for organic salts.[56]

The crystal structure of the cubic phase was investigated at 333 K by a crystal grown by slow solidification from the liquid state. Extinction rules suggest that the crystal belongs to the cubic space group *P*−43*n* or *Pm*−3*n*, which agrees with the powder XRD results. The diffraction image has only a

few spots in the low 2θ angle region (see Figure S25, Supporting Information, for an example of the diffraction images during the ω scan of 5° per frame). This observation suggests that the peaks in the region of high 2θ angle disappear because of the large atomic displacement factors of the constituent atoms. Although the structure was not fully solved and refined because of the highly disordered ions, the basic cation−anion configuration was obtained even in a rough form (see Table S4, Supporting Information, for detailed crystallographic data).

By considering the *FUV* at 273 K (563 $Å^3$), *V* at 333 K (3472 $Å^3$), and the lattice expansion, we determine *Z* of Phase I for $[P_4][PF_6]$ to be 6. However, a cubic structure with $Z = 6$ is not known for a simple inorganic 1:1 salt. When the centrosymmetric space group $Pm\bar{3}n$ is chosen, the three Wyckoff positions (6*b*, 6c, and 6*d*) have a multiplicity of 6. If the 6*b* site [(0,1/2,1/2), (1/2,0,1/2), (1/2,1/2,0), (0,1/2,0), (1/2,0,0), and (0,0,1/2)] is occupied by P_4^+ or PF_6^-, the counterion cannot occupy the 6*c* [(1/4,0,1/2), (3/4,0,1/2), (1/2,1/4,0), (1/2,3/4,0), (0,1/2,1/4), and (0,1/2,3/4)] or 6*d* [(1/4,1/2,0), (3/4,1/2,0), (0,1/4,1/2), (0,3/4,1/2), (1/2,0,1/4), and (1/2,0,3/4)] sites, because the 6*b* and 6*c* or 6*d* sites are too close to each other. Consequently, the only possible ion configuration is the one in which one ion occupies the 6*c* site and the other occupies the 6*d* site (Figure 7). The unit cell of Phase I for $[P_4][PF_6]$ is shown in Figure 8 (note that the ORTEP diagram is drawn at 5% probability). All the atoms have very large atomic displacement factors and the terminal carbon atom in the butyl group could not be determined. However, the unit cell diagram provides a clear idea of this structure in which the cation and anion are located on each face of the unit cell and the butyl chain is extended toward the (0, 0, 0) and (1/2, 1/2, 1/2) sites. This structure is called $TBPPF_6$-type here. As is clear from this model, isotropic rotation of the cation is ruled out in this structure.

Validity of the radius ratio rule. The radius ratio rules are introduced by considering the collision of the larger ions in ionic crystals.[57] Although the applicability of the radius ratio rules is limited from the viewpoint of structure prediction (especially for alkali metal halides), it is still useful for rough estimation of the effect of ion size on the crystal structure. According to these rules, the coordination number (CN) of a 1:1 salt is determined by the ratio of the radii of the cation and anion (r^+/r^-, where r^+ and r^- are the radii of the cation and anion, respectively ($r^+<r^-$)); CN = 3 for $0.155 < r^+/r^- < 0.225$, CN = 4 for $0.225 < r^+/r^- < 0.414$, CN = 6 for $0.414 < r^+/r^- < 0.732$, and CN = 8 for $0.732 < r^+/r^-$. Although the salts with non-spherical ions such as a complicated organic cation do not follow this rule, the ions in highly disordered structures often behave isotropically (or nearly isotropically), and can be treated as spherical. Therefore, the applicability of the radius ratio rule to Phase I of the present salts (CsCl'-type, NaCl-type, NaCl'-type, and inverse NiAs-type) is examined here (see Supporting Information for details of the following calculations). According to the radius ratio rule, a small r^-/r^+ results in the formation of a structure with a low CN such as the zinc blende-type if the ions behave spherically. However, the cations in the $TBPPF_6$-type structure are no longer regarded as spheres as shown above and thus the applicability is not examined here for this structural type.]

In order to estimate the radii of the ions in IPCs, we started from the assessment of the radius of PF_6^-, $r(PF_6^-)$, in the highly disordered structure. First, the $r(PF_6^-)$ value at 298 K in the highly disordered structure, $r(PF_6^-, 298\ K)$, is calculated from the PF_6^- salts $K[PF_6]$, $Rb[PF_6]$, and $Cs[PF_6]$.[58, 59] These three salts belong to the same $Cs[PF_6]$-type structure having the NaCl-type arrangement of ions, where the fluorine atoms in PF_6^- are disordered into 24 sites. The radii of the three alkali metal cations are available from the list of crystal radii by Shannon,[60] and the values for CN = 6 are chosen here as the NaCl-type structure ($r(K^+)$ = 1.52 Å, $r(Rb^+)$ = 1.66 Å, and $r(Cs^+)$ =1.81 Å). From this procedure, $r(PF_6^-, 298\ K)$ in IPC is estimated from lattice parameter a of the three salts (a = 7.7891(7) Å for $K[PF_6]$, a =

7.887(8) Å for Rb[PF_6] and a = 8.197(2) Å for Cs[PF_6]) according to the equation (1):

$$r(PF_6^-) = a/2 - r(M^+) \qquad (M^+ = K^+, Rb^+, \text{or } Cs^+) \qquad (1)$$

The three cases afford similar $r(PF_6^-, 298\ K)$ values (2.37 Å from K[PF_6], 2.28 Å from Rb[PF_6], and 2.29 Å for Cs[PF_6]), resulting in an averaged $r(PF_6^-)$ value of 2.31 Å. [61]

The radii of the other cations ($r(N_n^+)$ and $r(P_n^+)$) are calculated from lattice parameter a and $r(PF_6^-)$ according to equations (2), (3), and (4):

$$r(N_n^+) \text{ [or } r(P_n^+)] = a/2 - r(PF_6^-) \qquad \text{(NaCl- and NaCl'-type lattice)} \qquad (2)$$

$$r(N_n^+) \text{ [or } r(P_n^+)] = 3^{1/2} \cdot a/2 - r(PF_6^-) \qquad \text{(CsCl'-type lattice)} \qquad (3)$$

Table 3 Structural types, radii of the ions and the radius ratio of the cation and anion for Phase I of selected [N_n][BF_4], [N_n][PF_6], [P_n][BF_4], and [P_n][PF_6][a]

	Structural type	r^+ / Å	r^- / Å	r^-/r^+
[N_1][PF_6]	CsCl' at 563 K (CN = 8)	3.14	2.37	0.74
[N_2][BF_4]	NaCl at 373 K (CN = 6)	3.34	2.07	0.62
[N_2][PF_6]	NaCl at 373 K (CN = 6)	3.34	2.37	0.69
[P_2][BF_4]	NaCl at 473 K (CN = 6)	3.61	2.07	0.57
[P_2][PF_6]	NaCl at 498 K (CN = 6)	3.61	2.37	0.64
[N_3][PF_6]	NaCl' at 493 K (CN = 6)	3.71	2.37	0.62
[P_3][PF_6]	Inverse-NiAs at 473 K (CN = 6)	4.16	2.37	0.56

[a] r^+, r^-, and CN denote the radii of the cation and anion and coordination number, respectively.

$$r(N_n^+)\ [\text{or } r(P_n^+)] = [(a/3^{1/2})^2 + (c/4)^2]^{1/2} - r(PF_6^-) \quad \text{(inverse NiAs-type lattice)} \qquad (4)$$

It should be noted that parameter a in equation (2) is half that for the CsCl'-type structure, as described above.

The radius of BF_4^-, $r(BF_4^-)$, is then calculated from lattice parameter a and $r(N_n^+)$ [or $r(P_n^+)$] by analogy with equation (2).

The calculated radii and resulting radius ratios of the present salts are listed in Table 3 (note that $r^- < r^+$ in the present cases). The radius ratio rule described above is applied appropriately to all the salts with the CsCl'-type structure ($[N_1][PF_6]$), NaCl-type structure ($[N_2][BF_4]$, $[N_2][PF_6]$, $[P_2][BF_4]$, and $[P_2][PF_6]$), NaCl'-type structure ($[N_3][PF_6]$) and inverse NiAs-type structure ($[P_3][PF_6]$), although attention should be paid to the CsCl'-type and NaCl'-type structures owing to the limitation in the spherical model for the ions therein.

Conclusions

The present systematic study by X-ray diffraction techniques revealed that the highly disordered structures of symmetric tetraalkylammonium (N_n^+) and tetraalkylphosphonium (P_n^+) salts ($[N_n][BF_4]$, $[N_n][PF_6]$, $[P_n][BF_4]$, and $[P_n][PF_6]$, where n = 1 to 4,) are classified into 5 different types: CsCl', NaCl, NaCl', inverse NiAs, and $TBPPF_6$. The effect of ion size on the structural type is interpreted by estimating the radius ratio of the cation and anion. Validity of the radius ratio rules was shown in the cases of the highly symmetric cations, whereas the cations with long alkyl chains but cannot be regarded

as spheres even in a highly disordered cubic structure. The information obtained in this study should aid in experimental and computational modeling of organic IPC materials.

Acknowledgements

The authors would like to thank The Kyoto Technoscience Center for their financial support to this work.

References

1. T. G. Coker, J. Ambrose and G. J. Janz, *J. Am. Chem. Soc.*, 1970, **92**, 5293-5297.
2. G. Zabinska, P. Ferloni and M. Sanesi, *Thermochim. Acta*, 1987, **122**, 87-94.
3. G. Zabinska, P. Ferloni and M. Sanesi, *Thermochim. Acta*, 1988, **137**, 39-49.
4. J. Levkov, W. Kohr and R. A. Mackay, *J. Phys. Chem.*, 1971, **75**, 2066-2069.
5. M. Herstedt, W. A. Henderson, M. Smirnov, L. Ducasse, L. Servant, D. Talaga and J. C. Lassegues, *J. Mol. Struct.*, 2006, **783**, 145-156.
6. W. H. J. Debeer, A. M. Heyns, P. W. Richter and J. B. Clark, *J. Solid State Chem.*, 1981, **36**, 171-178.
7. A. Xenopoulos, A. H. Narten, J. L. Cheng and B. Wunderlich, *J. Non-Cryst. Solids*, 1991, **131**, 113-119.
8. H. Ono, R. Ikeda and H. Ishida, *Ber. Bunsen Phys. Chem.*, 1996, **100**, 1833-1838.

9. V. Armel, D. Velayutham, J. Z. Sun, P. C. Howlett, M. Forsyth, D. R. MacFarlane and J. M. Pringle, *J. Mater. Chem.*, 2011, **21**, 7640-7650.

10. H. Yoon, G. H. Lane, Y. Shekibi, P. C. Howlett, M. Forsyth, A. S. Best and D. R. MacFarlane, *Energy Environ. Sci.*, 2013, **6**, 979-986.

11. D. R. MacFarlane and M. Forsyth, *Adv. Mater.*, 2001, **13**, 957-966.

12. J. M. Pringle, P. C. Howlett, D. R. MacFarlane and M. Forsyth, *J. Mater. Chem.*, 2010, **20**, 2056-2062.

13. J. M. Pringle, *Phys. Chem. Chem. Phys.*, 2013, **15**, 1339-1351.

14. D. R. MacFarlane, J. H. Huang and M. Forsyth, *Nature*, 1999, **402**, 792-794.

15. E. I. Cooper and C. A. Angell, *Solid State Ionics*, 1986, **18-9**, 570-576.

16. Y. Abu-Lebdeh, P. J. Alarco and M. Armand, *Angew. Chem. Int. Ed.*, 2003, **42**, 4499-4501.

17. S. Iwai, M. Hattori, D. Nakamura and R. Ikeda, *J. Chem. Soc., Faraday Trans.*, 1993, **89**, 827-831.

18. T. Shimizu, S. Tanaka, N. OnodaYamamuro, S. Ishimaru and R. Ikeda, *J. Chem. Soc., Faraday Trans.*, 1997, **93**, 321-326.

19. T. Tanabe, D. Nakamura and R. Ikeda, *J. Chem. Soc., Faraday Trans.*, 1991, **87**, 987-990.

20. K. Kuchitsu, H. Ono, S. Ishimaru, R. Ikeda and H. Ishida, *Phys. Chem. Chem. Phys.*, 2000, **2**, 3883-3885.

21. P. J. Alarco, Y. Abu-Lebdeh and M. Armand, *Solid State Ionics*, 2004, **175**, 717-720.

22. P. J. Alarco, Y. Abu-Lebdeh, N. Ravet and M. Armand, *Solid State Ionics*, 2004, **172**, 53-56.

23. L. Y. Jin, K. M. Nairn, C. M. Forsyth, A. J. Seeber, D. R. MacFarlane, P. C. Howlett, M. Forsyth and J. M. Pringle, *J. Am. Chem. Soc.*, 2012, **134**, 9688-9697.

24. D. R. MacFarlane, P. Meakin, J. Sun, N. Amini and M. Forsyth, *J. Phys. Chem. B*, 1999, **103**, 4164-4170.

25. W. A. Henderson, M. Herstedt, V. G. Young, S. Passerini, H. C. De Long and P. C. Trulove, *Inorg. Chem.*, 2006, **45**, 1412-1414.

26. W. A. Henderson, V. G. Young, S. Passerini, P. C. Trulove and H. C. De Long, *Chem. Mater.*, 2006, **18**, 934-938.

27. S. Forsyth, J. Golding, D. R. MacFarlane and M. Forsyth, *Electrochim. Acta*, 2001, **46**, 1753-1757.

28. J. Golding, N. Hamid, D. R. MacFarlane, M. Forsyth, C. Forsyth, C. Collins and J. Huang, *Chem. Mater.*, 2001, **13**, 558-564.

29. J. Timmermans, *J. Phys. Chem. Solids*, 1961, **18**, 1-8.

30. H. Ishida, T. Iwachido and R. Ikeda, *Ber. Bunsen Phys. Chem.*, 1992, **96**, 1468-1470.

31. H. Ishida, Y. Furukawa, S. Kashino, S. Sato and R. Ikeda, *Ber. Bunsen Phys. Chem.*, 1996, **100**, 433-439.

32. H. Ishida, S. Kashino and R. Ikeda, *Z. Naturforsch A*, 2000, **55**, 765-768.

33. K. Matsumoto, T. Okawa and R. Hagiwara, *Chem. Lett.*, 2012, **41**, 394-396.

34. H. Ishida, Y. Kubozono, S. Kashino and R. Ikeda, *Z. Naturforsch A*, 1994, **49**, 723-726.

35. W. J. Dunning, *J. Phys. Chem. Solids*, 1961, **18**, 21-27.

36. W. A. Henderson, V. G. Young, Jr., W. Pearson, S. Passerini, H. C. De Long and P. C. Trulove, *J. Phys.: Condens. Matter*, 2006, **18**, 10377-10390.

37. C. M. Forsyth, D. R. MacFarlane, J. J. Golding, J. Huang, J. Sun and M. Forsyth, *Chem. Mater.*, 2002, **14**, 2103-2108.

38. J. M. Pringle, J. Adebahr, D. R. MacFarlane and M. Forsyth, *Phys. Chem. Chem. Phys.*, 2010, **12**, 7234-7240.

39. G. Giuseppetti, F. Mazzi, C. Tadini, P. Ferloni, G. Zabinska and S. Torre, *Z. Kristallogr.*, 1997, **212**, 367-371.

40. G. Giuseppetti, F. Mazzi, C. Tadini, P. Ferloni and S. Torre, *Z. Kristallogr.*, 1992, **202**, 81-88.

41. H. Ishida, T. Nakai, N. Kumagae, Y. Kubozono and S. Kashino, *J. Mol. Struct.*, 2002, **606**, 273-279.

42. J. C. W. Folmer, R. L. Withers, T. R. Welberry and J. D. Martin, *Phys. Rev. B*, 2008, **77**.

43. A. Boultif and D. Louer, *J. Appl. Crystallogr.*, 2004, **37**, 724-731.

44. RAPID AUTO 2.40, Rigaku Corporation, Tokyo, Japan, 2006.

45. A. Altomare, G. Cascarano, C. Giacovazzo and A. Guagliardi, *J. Appl. Crystallogr.*, 1993, **26**, 343-350.

46. G. M. Sheldrick, *Acta. Crystallogr. A*, 2008, **64**, 112-122.

47. L. J. Farrugia, *J. Appl. Crystallogr.*, 1999, **32**, 837-838.

48. M. R. R. Prasad, K. Krishnan, K. N. Ninan and V. N. Krishnamurthy, *Thermochim. Acta*, 1997, **297**, 207-210.

49. C. M. Wheeler and R. A. Sandstedt, *J. Am. Chem. Soc.*, 1955, **77**, 2025-2026.

50. Although the DSC curve of $[P_1][BF_4]$ showed 2 distinct endothermic peaks, XRD patterns below and above these transition temperatures were not different very much. This may result from two reasons; the structural changes are too small to detect or the structural changes did not occur during the XRD measurement because of slow dynamics.

51. Y. Wang, L. D. Calvert and S. K. Brownstein, *Acta Crystallogr. B*, 1980, **36**, 1523-1523.

52. K. O. Christe, W. W. Wilson, R. D. Wilson, R. Bau and J. A. Feng, *J. Am. Chem. Soc.*, 1990, **112**, 7619-7625.

53. T. Enomoto, S. Kanematsu, K. Tsunashima, K. Matsumoto and R. Hagiwara, *Phys. Chem. Chem. Phys.*, **13**, 12536-12544.

54. R. Asayama, J. Kawamura and T. Hattori, *Chem. Phys. Lett.*, 2005, **414**, 87-91.

55. Z. Stein and I. Goldberg, *Acta Crystallogr. E*, 2005, **61**, O272-O274.

56. W. Beichel, U. P. Preiss, B. Benkmil, G. Steinfeld, P. Eiden, A. Kraft and I. Krossing, *Z. Anorg. Allg. Chem.*, 2013, **639**, 2153-2161.

57. P. Atkins, T. Overton, J. Rourke, M. Weller and F. Armstrong, *Shriver & Atkins Inorganic Chemistry, Oxford University Press, Oxford, 2006.*

58. K. Kitashita, R. Hagiwara, Y. Ito and O. Tamada, *J. Fluorine Chem.*, 2000, **101**, 173-179.

59. Z. Mazej and R. Hagiwara, *J. Fluorine Chem.*, 2007, **128**, 423-437.

60. R. D. Shannon, *Acta. Crystallogr. A*, 1976, **32**, 751-767.

61. The resulting $r(Cs^+)/r(PF_6^-)$ is 0.78, which exceeds the upper limit for CN = 6 (0.732). Given that the radius ratio rules are applicable to $Cs[PF_6]$, this indicates that $r(Cs^+)$ and $r(PF_6^-)$ are slightly overestimated and underestimated, respectively.